Factors Affecting Silicon Membrane Burst Strength

Albert K. Henning, Sapna Patel, Michael Selser, and Bradford A. Cozad
Redwood Microsystems, 959 Hamilton Avenue, Menlo Park, CA USA 94025

ABSTRACT

Factors affecting the fracture strength of single-crystal silicon membranes are assessed. These factors include: membrane shape at the membrane's intersection with structural frames or sidewalls, membrane thickness, membrane surface roughness, membrane mis-orientation to the principal crystallographic axes, wafer starting material quality, membrane stress (or pre-tension), and microstructure and shape at bond interfaces, such as the anodic bond interface between membrane and Pyrex wafers. Measurements of fracture strength versus these factors are made. Direct measurements of stress are also made using micro-Raman techniques. Simulations of membrane structures are studied, in order to evaluate the measurements. The results indicate that the predominant factor affecting fracture strength is surface roughness.

1. INTRODUCTION

Microfabricated membranes or diaphragms constructed from single-crystal silicon are found in a number of applications. Of particular interest are microvalves utilizing membranes to modulate flow [1,2]. Also of interest are membranes, or thin single-crystal silicon beams, used in micropumps [3], pressure sensors [4,5], accelerometers [6], and acoustic (sound) receivers or generators [7,8].

Previous work has looked at fracture of single-crystal silicon structures in both membrane and non-membrane configurations. The dependence of yield strength on crystal orientation has been studied [9,10]. Very substantial variation from the ideal value for bulk silicon in the <100> direction (7 GPa [11]) were observed, with certain orientations yielding to fracture at stress values as low as 0.6 GPa. The effects of plasma etching have been examined, including effects on surface roughness [12] and moisture [13]. Data suggested that environmental effects, such as moisture, did not play a role in crack generation and propagation [13]. Other work has also examined the effect of surface roughness caused by plasma etching [14]. Beyond the sudden or fast processes studied here, slow-velocity effects have also been studied [15]. The unexpected effect of reflected mechanical waves on fracture topology has been postulated and confirmed through measurement [16].

In this work, a variety of factors affecting the fracture strength of single-crystal silicon membranes are assessed. These factors include: membrane shape at the intersection between membrane, and structural frames or sidewalls; membrane thickness; membrane surface roughness; membrane mis-orientation to the principal crystallographic axes [9,10]; wafer starting material; membrane stress; and microstructure and shape at the membrane-Pyrex anodic bond interface [17]. Measurements of fracture strength versus these factors are made. Direct measurements of stress are also made [18]. Simulations of membrane structures are studied, including the effect of a boss in the membrane, in order to evaluate the measurements.

Cycling effects, such as ultra-low velocity crack propagation [15], creep, or long-term defect nucleation due to repeated stress, are not considered here.

2. THEORY

Simple membrane theory can be used to develop an initial set of expectations for the development of stress in single-crystal silicon membranes. The deflection of such a membrane, as a function of transmembrane pressure, is given by [19]:

Reliability, Testing, and Characterization of MEMS/MOEMS III, edited by
Danelle M. Tanner, Rajeshuni Ramesham, Proceedings of SPIE Vol. 5343
(SPIE, Bellingham, WA, 2004) · 0277-786X/04/$15 · doi: 10.1117/12.524648

$$\frac{Pa^4}{Eh^4} = A\frac{y}{h} + B\frac{y^3}{h^3} \quad (1)$$

P is the transmembrane pressure, a is the length of the side of a square membrane, E is the Young's modulus for the membrane material, and h is the membrane thickness. A and B are constants related to Poisson's ratio, membrane structural parameters, and initial membrane stress. y is the deflection of the center of the membrane. This formulation ignores the fact that silicon's mechanical properties are not isotropic with respect to crystal direction, but is more than sufficient to understand and predict the mechanical behavior.

The maximum stress which develops as a result of this deflection is given by:

$$\sigma = \beta P \frac{a^2}{h^2} \quad (2)$$

where the leading coefficient has a value of about 0.31 for a square membrane. Note that in this formulation the stress will be linear in the transmembrane pressure, but cubic in the deflection of the membrane center. Also, the peak stress will occur at the center of each of the four sides of the membrane, where it is assumed to be clamped rigidly to the frame. In actual devices, and in finite element simulations, the relationship between peak stress and transmembrane pressure will not be exactly linear, as will be shown.

3. MECHANISMS AND THEIR EVALUATION

The silicon membranes used in microvalves for this study are nominally 50 µm thick, and 4.5 mm in square extent. KOH anisotropic etching defines the membranes from both top and bottom side of the wafer, so that the membranes are ideally oriented to the <100> silicon crystallographic direction which gives the highest fracture, or burst strength. The KOH etch may or may not be followed by an HF:nitric acid:acetic acid etch, which rounds the membrane at the critical points of peak stress versus deflection, creating a fillet.

During processing, the membranes are tested for burst, or fracture, strength, as a function of applied transmembrane pressure. A variety of mechanisms were considered, and are assessed as follows.

3.1 Effect of directionality of applied pressure

Directionality of applied pressure was considered. The membranes studied here are KOH- and fillet-etched from both sides, creating a stair-step effect (Figure 1), such that the membrane edge on one etched side does not align top to bottom with the edge on the reverse side (but is still parallel to it). In such a structural configuration, it seemed plausible that the mechanism of stress loading and fracture would depend on the direction of the applied transmembrane pressure.

ANSYS was used to explore the effect. Figure 2 shows the two situations which were studied. The simulations were two-dimensional in nature, but the results were expected to hold true qualitatively for actual three-dimensional structures. In the simulations, a transmembrane pressure of 700 kPa was applied. The resulting stress contours were mapped, and the peak stress was noted. The results showed that the reverse configuration(that is, pressure applied from bottom to top in Figure 2) produced a peak stress 40% less than that for the forward direction. Subsequently, measurements on actual membranes confirmed a 30% difference. However, this difference was not enough to account for the more than 10X reduction in burst strength observed in manufactured structures.

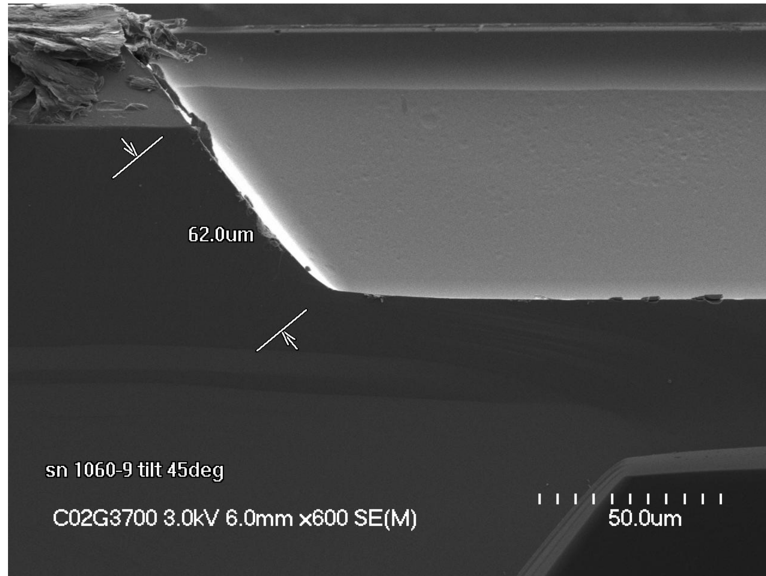

Figure 1: Cross-section of a membrane which was been subjected to both KOH and fillet etching (note the rounded interface between the sloped sidewalls and the flat membrane).

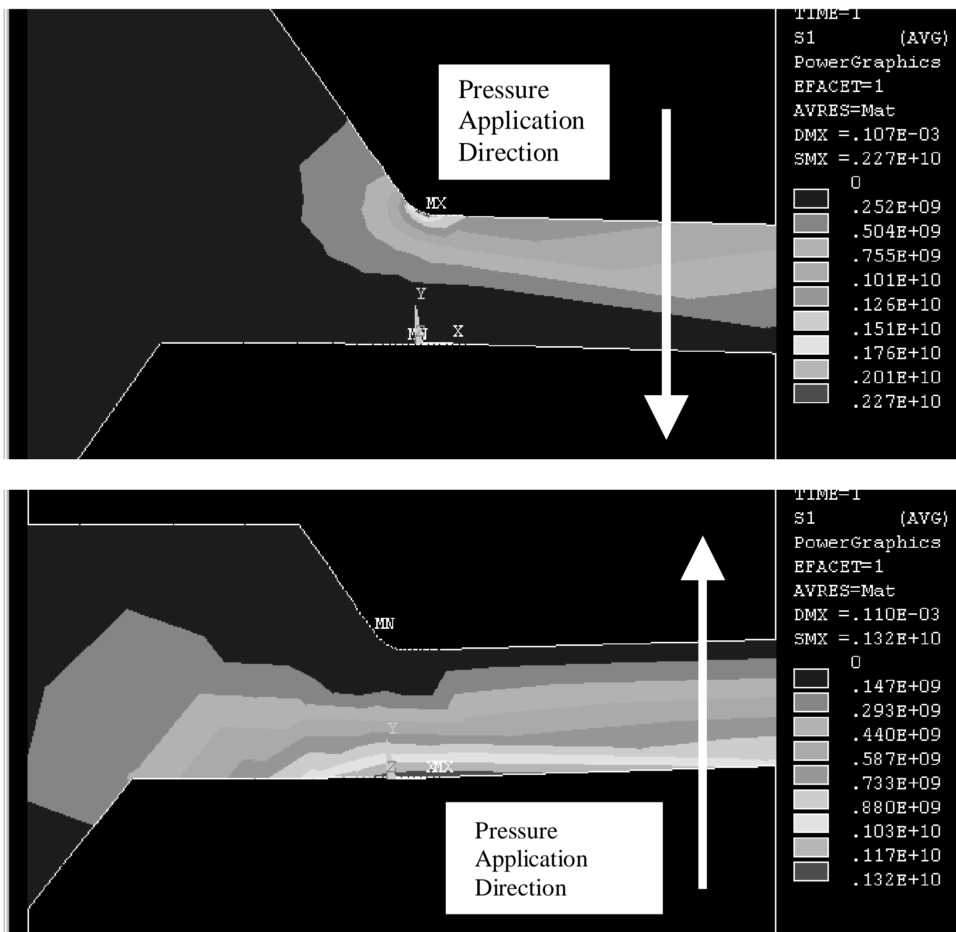

Figure 2: Effect of forward (upper) and reverse (lower) pressure application on membrane stress and fracture. ANSYS simulation shown. (Note that the simulated structure is flipped from the actual structure depicted in Figure 1).

3.2 Effect of surface roughness

Surface roughness effects, caused by the two wet chemical etching processes, were considered. Membranes similar to that shown in Figure 3 were created. Deliberate roughening of the membrane surfaces was effected, by making adjustments to the KOH etch and the fillet etch processes.

Characterization involved correlating SEM-based measurements of surface roughness (using SEM photomicrographs such as those shown in the lower portions of Figure 3) with measurements of burst strength. The results are shown in Figure 4. The plateau at the smallest values of surface roughness (surface roughness less than ~ 100 nm), where the transmembrane pressure is 600 psid, corresponds to a value of maximum membrane stress between 1.3 and 2.0 GPa, as determined using either analytical theory or ANSYS simulation, and depending upon which manifestation of stress (e.g. S1) is inspected. This value range compares to the measurement of 1.0 GPa reported in [14]. All values, however, are substantially below the theoretical maximum of 7.0 GPa.

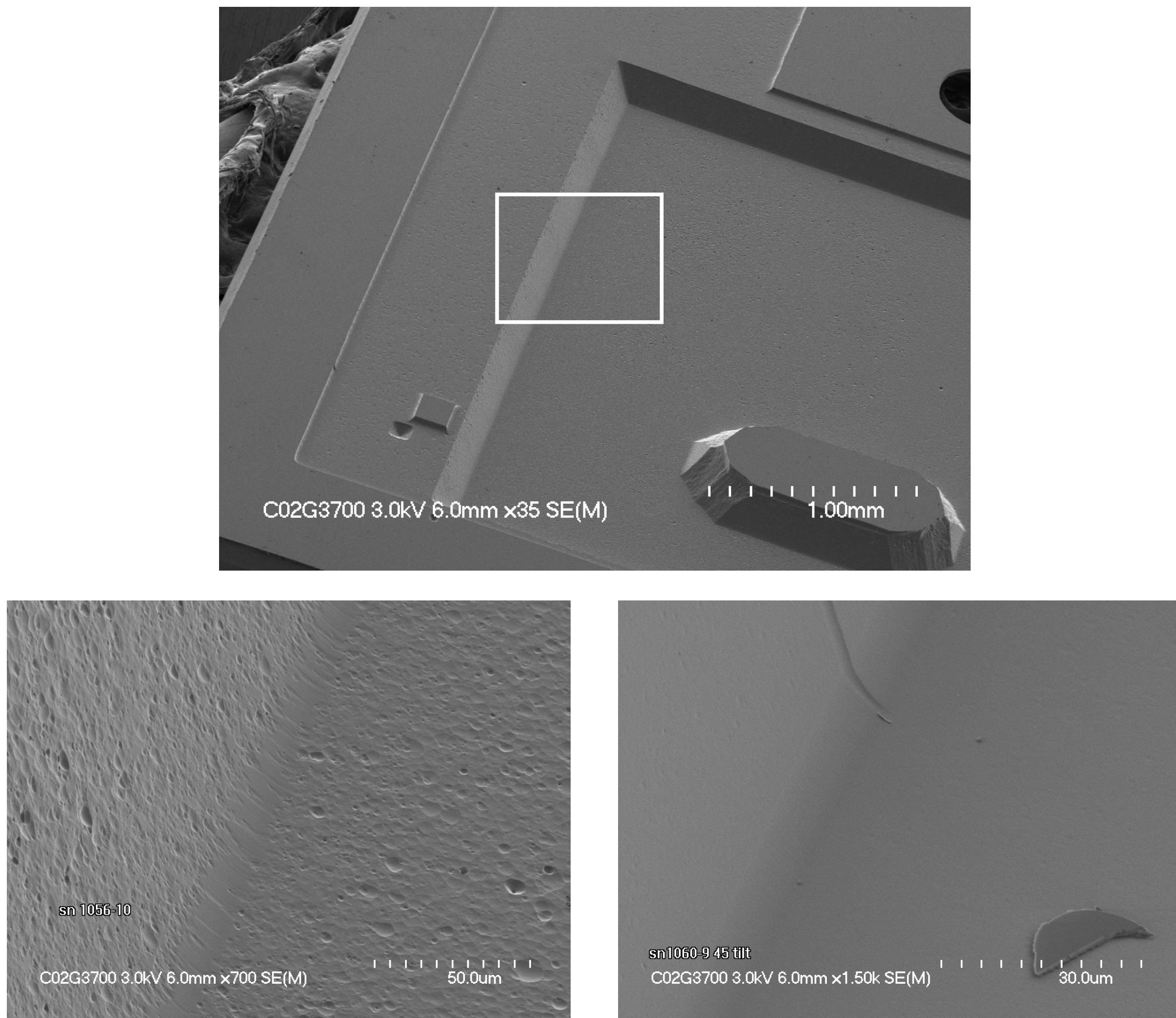

Figure 3: SEMS of membranes used in the surface roughness study. Top: Primary membrane structure studied. The field of view for the high magnification SEMs is also shown. (Note that the presence of the boss structure, located in the lower right of the SEM photomicrograph, did not substantial alter the yield strength results.) Lower left: A rough surface, achieved as a result of wet chemical etching. Lower right: A smooth surface, also achieved as a result of wet chemical etching.

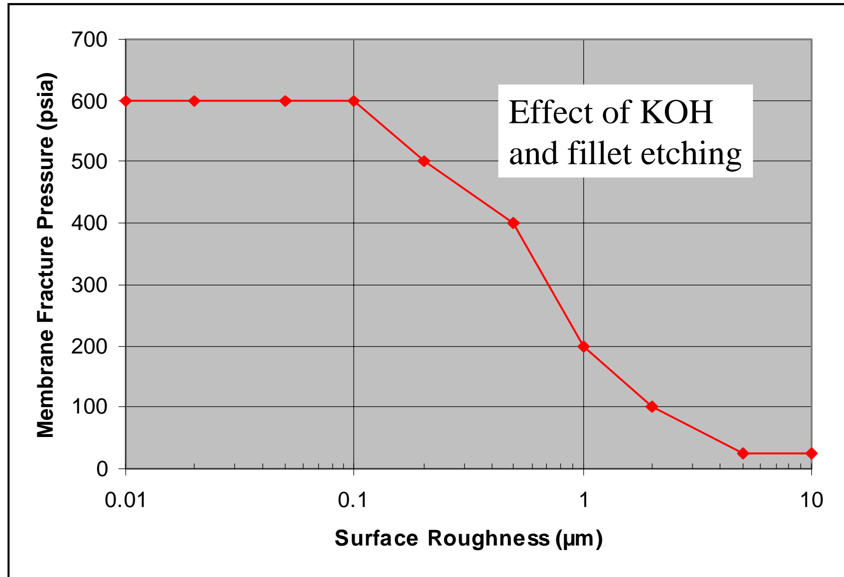

Figure 4: The effect of surface roughness, caused by wet etching, and membrane fracture strength.

3.3 Effect of Pyrex-silicon delamination

The effect of delamination between the microvalve Pyrex and silicon membrane layers was studied (Figure 5) [17]. In this instance, membrane fracture *per se* does not occur. Instead, the interface between the silicon membrane and the Pyrex wafer is stressed. The interface occurs due to anodic bonding between the Pyrex and silicon layers. As can be seen in Figure 5, this delamination effect is predicted to occur around 3.8 MPa or 580 psid, which is comparable to the best observed membrane fracture of 600 psid. As a consequence, while this failure mechanism is important, the membrane fracture presents a more stringent limit in terms of actual manufacturing.

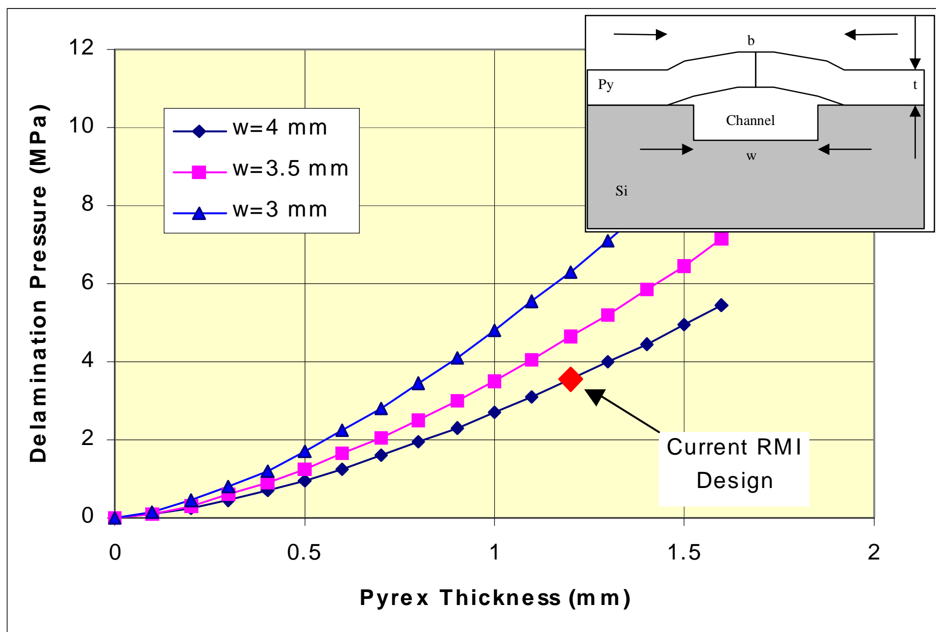

Figure 5: Modeling the effect of Pyrex-silicon delamination (after [17]).

3.4 Effect of wafer mis-orientation

In order to assess a practical manufacturing attribute, the mis-alignment of the fabricated membrane structure to the crystallographic wafer orientation was measured, and compared to burst strength data. Figure 6 shows schematically the two wafer mis-orientation effects which were studied. Table 1 shows the data on burst strength vs. mis-orientation which was measured. While the number of samples was small, no readily identifiable correlation was observed, leading to closer examination of other mechanisms.

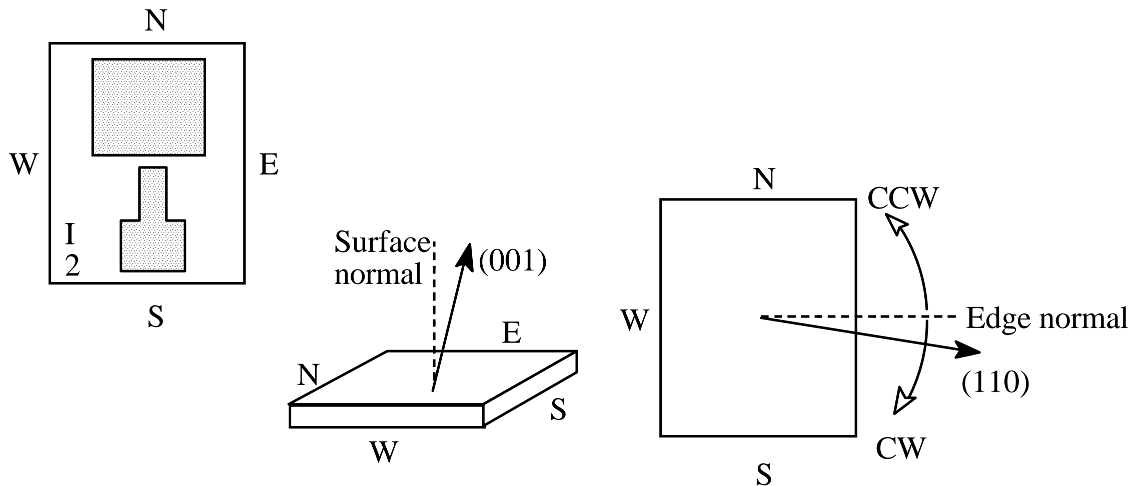

Figure 6: Schematics of the two wafer mis-orientation effects studied.

Sample	Burst Strength (psi)	<100> Misorientation	<010> Misorientation
1058-3	55	0.15° W, 0.10°N	-0.7° (CCW)
1058-4	302	0.75° E, 0.07°N	0.35° (CW)
1058-7	131	0.05° W, 0.20°S	0.25° (CW)

Table 1: Effects of wafer mis-orientation on membrane fracture strength.

3.5 Effect of membrane edge radius of curvature

Figures 1 and 2 depicted, in part, the structure at the membrane-frame interface. In order to understand the effect of the radius of curvature at this interface, ANSYS simulation was used. Three structures were examined. The first had a 15 µm radius of curvature. The second had a sharp interface, representative of the absence of fillet etch, and a zero-value radius of curvature. The third had an intentional notch feature, to represent the type of stress concentration which a defect or asperity might contribute. The results of the simulation are shown in Figure 7. As expected, a notch concentrates the bending energy in a smaller volume, leading to higher stress, while a non-zero radius of curvature distributes the stored bending energy in a larger volume, resulting in lowered stress.

Table 2 shows measurements of radius of curvature versus measured fracture or burst strength. The absence of a clear correlation strongly suggests another cause, such as surface roughness, must be present.

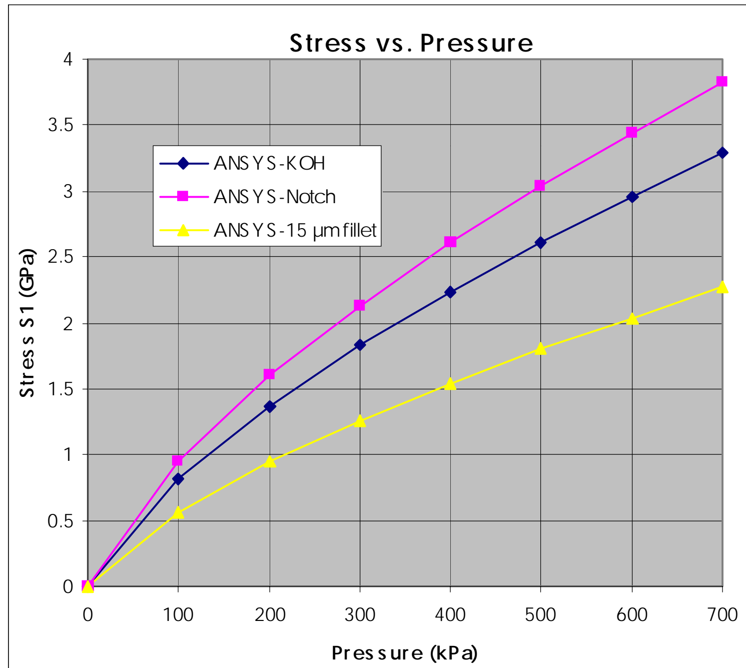

Figure 7: ANSYS simulation of effect on peak membrane stress of radius of curvature structure at membrane-frame boundary. Note that, contrary to Equation (2), stress is not exactly linear in pressure. The ANSYS simulation includes non-linear effects, and correctly predicts the cubic dependence of pressure on deflection given by Equation (1).

Sample	Radius (µm)	Burst Strength (psig)
1053-6 (SOV)	17.6	314
1058-7 (SOV)	17.3	131
1060-9 (SOV)	9.1	> 300
1056-7 (SOV)	12.5	106
1058-3 (SOV)	16.3	55

Table 2: Radius of curvature versus membrane fracture strength.

3.6 Other effects and measurements

Stress versus transmembrane pressure was measured directly, using micro-Raman spectroscopy [19]. Figure 8 shows the results of this measurement, for a membrane with a uniform pressure load and a center deflection of approximately 53 µm. The instrument is looking at the concave side of the membrane, so that the center stress is identified as compressive, while the stress near the edge is more tensile in nature. The measured membrane structure is bonded to a Pyrex layer, which may explain the compressive stress condition beyond the intersection between the membrane and the frame. Alternatively, the compression measured at the right of Figure 8 may be an artifact arising from the non-orthogonal nature of the incident laser light with the angled, KOH-etched sidewall.

Other effects, such as Czochralski (CZ) vs. float-zone (FZ) starting material, were also studied. Czochralski material is well known to include clusters of defects related to high, non-uniform concentrations of oxygen, while float-zone material removes many such defects. Typically, no substantial distinction has been made in the microelectronics community between CZ and FZ material properties related to electronic transport. However, since gettering techniques are always employed, to remove defects from the electronically-active, surface portions of microelectronic devices, it is not clear what the point defect structure will be well into the bulk of the material. Nor is it clear how these point defects may affect mechanical properties, such as fracture strength, crack propagation, creep, and long-term cycling behavior.

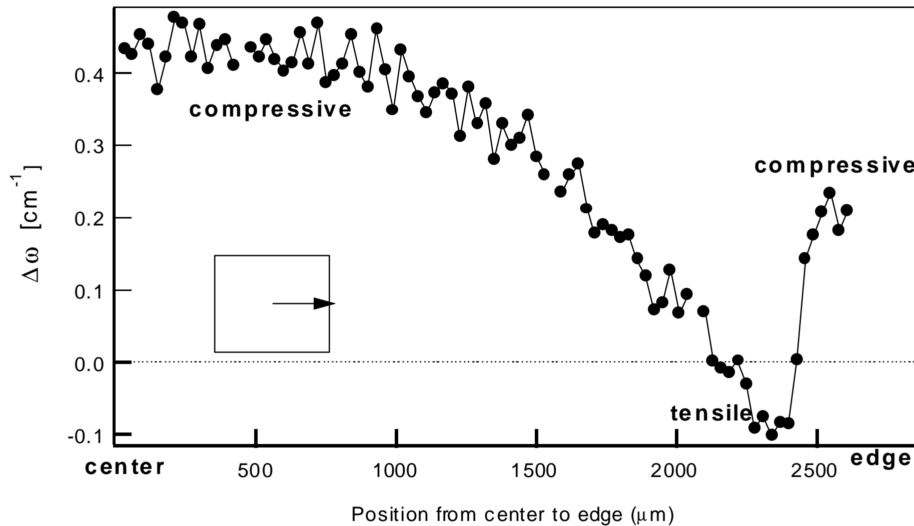

Figure 8: micro-Raman measurement of stress in deflected membrane. 0.44 on the *y*-axis scale corresponds to a stress value of –190 MPa. (Courtesy I. DeWolf, IMEC.)

3. DISCUSSION

The work presented herein suggests strongly that, regardless of the etch process used to define a micromechanical structure, the surface roughness is the most important attribute to control, in order to maintain high yield strengths, and to achieve devices with the most robust mechanical reliability.

However, this result, though important, is incomplete. Others have reported related observations. The work of Ref. [14] gave evidence of fracture versus roughness, but at values of roughness less than the saturation value shown in Figure 2 above. Also, the work of Ref. [20] incorporates surface roughness into a phenomenological model of fracture and reliability, but the data supporting the model is not disclosed, at least not for silicon.

What is not known is the underlying mechanism which couples surface roughness to fracture. Does the roughness merely expose lower energy crystalline fracture planes? Or, does the roughness nucleate or modulate chemico-mechanical structures (through an interaction between local stress and local voids or other point defect concentrations) which lower the energy threshold for fracture? Or, is the roughness merely evidence of a bulk contamination, which creates both pre-tension and stress, while simultaneously causing etch variations which decorate the stress? The exact answer to these questions is not yet known, and must be the subject of further investigation.

4. CONCLUSIONS

Fracture strength is an important attribute of silicon membranes used in microdevices. In this work, we have examined a variety of attributes, which may contribute to the premature fracture of silicon membranes subjected to pressure loading. The most dominant cause by far, which correlates to low fracture pressures, is the surface microroughness caused by wet etching. This result is consistent with observations in dry etching environments. What remains to be determined is whether the surface microroughness is caused directly by the etch process, or is an indirect manifestation of other causes, such as high concentrations of point defects in the bulk or surface silicon, or a pre-stressed condition in the membrane itself.

REFERENCES

1. M. J. Zdeblick and J. B. Angell, "A microminiature electric-to-fluidic valve." In Proceedings, *Transducers '87 (1987 Int'l. Conf. Sol. State Sens. and Act.)*, pp. 827-830 (IEEE, Piscataway, NJ, 1987).
2. P. W. Barth, "Silicon microvalves for gas flow control." In Proceedings, *Transducers '95 (1995 Int'l. Conf. Sol. State Sens. and Act.)*, pp. 276-279 (IEEE, Piscataway, NJ, 1995).
3. P. Woias, "Micropumps: summarizing the first two decades." In Proceedings, *Microfluidics and BioMEMS*, vol. 4560, pp. 39-52 (SPIE, Bellingham, WA, 2001; C. H. Mastrangelo and H. Becker, eds).
4. O. N. Tufte, P. W. Chapman, and D. Long, "Silicon diffused-element piezoresistive diaphragms." *J. Appl. Phys.* **33**, p. 3322 (1962).
5. A. K. Henning, A. Zias, N. Mourlas, and S. Metz, "A MEMS-based, high-sensitivity pressure sensor for ultraclean semiconductor applications." In Proceedings, *13th IEEE/SEMI Advanced Semiconductor Manufacturing Conference and Workshop (ASMC)*, pp. 165-168 (IEEE, Piscataway, NJ, 2002).
6. L. M. Roylance and J. B. Angell, "A batch fabricated silicon accelerometer." *IEEE Trans. Electron Dev.*, **ED-26**(12), pp. 1911-1916 (1979).
7. Y. B. Ning, A. W. Micthell, and R. N. Tait, "Fabrication of a silicon micromachined capacitive microphone using a dry-etch process." *Sens. and Act.* **A53**, pp. 237-242 (1996).
8. J. J. Neumann and K. J. Gabriel, "CMOS-MEMS membrane for audio-frequency acoustic actuation." *Sens. and Act.* **A95**, pp. 175-182 (2002).
9. C. J. Wilson and P. A. Beck, "Fracture testing of bulk silicon microcantilever beams subjected to a side load." *J-MEMS* **5**(3), pp. 142-150 (1996).
10. L. Li, T. Yi, and C.-J. Kim, "Effect of mask-to-crystal direction misalignment on fracture strength of silicon microbeam." In Proceedings, *Microscale Systems: Mechanics and Measurements Symposium*, pp. 36-40 (Society for Experimental Mechanics, Bethel, CT, 2000).
11. K. E. Petersen, "Silicon as a mechanical material." *Proc. IEEE* **70**(5), pp. 420-457 (1982).
12. A. M. Fitzgerald, R. H. Dauskardt, and T. W. Kenny, "Fracture toughness and crack growth phenomena of plasma-etched single crystal silicon." *Sens. and Act.* **A83**, pp. 194-199 (2000).
13. A. M. Fitzgerald, R. S. Iyer, R. H. Dauskardt, and T. W. Kenny, "Subcritical crack growth in single-crystal silicon using micromachined specimens." *J. Mater. Res.* **17**, pp. 683-692 (2002).
14. K.-S. Chen, A. A. Ayón, X. Zhang and S. M. Sperling, "Effect of process parameters on the surface morphology and mechanical performance of silicon structures after deep reactive ion etching (DRIE)." *J-MEMS* **11**(3), pp. 264-275 (2002).
15. C. L. Muhlstein, S. B. Brown, and R. O. Ritchie, "High-cycle fatigue in single-crystal silicon thin films." *J-MEMS* **10**(4), pp. 593-600 (2001).
16. Alissa M. Fitzgerald, "Crack growth phenomena in micro machined single crystal silicon and design implications for micro electro mechanical systems (MEMS)." Ph.D. dissertation, Stanford University (Stanford, CA, 2000).
17. M. T. Blom, N. R. Tas, G. Pandraud, E. Chmela, J. G. E. Gardeniers, R. Tijssen, M. Elwenspoek, and A. van den Berg, "Failure mechanisms of pressurized microchannels: model and experiments." *J-MEMS* **10**(1), pp. 158-164 (2001).
18. I. De Wolf, G. Pozzat, K. Pinardl, D. J. Howard, M. Ignat, S. C. Jain, and H. E. Maes, "Experimental validation of mechanical stress models by micro-Raman spectroscopy." In Proceedings, *7th European Symposium on Reliability of Electron Devices, Failure Physics and Analysis*, pp. 1751-1754 (IEEE, Piscataway, NJ, 1996).
19. Mario Di Giovanni, Flat and Corrugated Diaphragm Design Handbook. (Marcel Dekker, New York, NY, 1982).
20. N. N. Nemeth, L. M. Powers, L. A. Janosik, and J. P. Gyekenyesi, "Lifetime reliability evaluation of structural ceramic parts with the CARES/LIFE computer program." In Proceedings, *34th AIAA/ASME/ASCE/ASC Structures, Structural Dynamics, and Materials Conference*, pp. 1634-1646 (American Institute for Aeronautics and Astronautics, Washington, D.C., 1993).